Photonic implementation of a neuronal algorithm applicable towards angle of arrival detection and localization

Ryan Toole and Mable P. Fok*

Lightwave and Microwave Photonic Laboratory, College of Engineering, The University of Georgia, Athens, Georgia, 30602, USA

**mfok@uga.edu*

Abstract: A photonic system exemplifying the neurobiological learning algorithm, spike timing dependent plasticity (STDP), is experimentally demonstrated using the cooperative effects of cross gain modulation and nonlinear polarization rotation within an SOA. Furthermore, an STDP-based photonic approach towards the measurement of the angle of arrival (AOA) of a microwave signal is developed, and a three-dimensional AOA localization scheme is explored. Measurement accuracies on the order of tens of centimeters, rivaling that of complex positioning systems that utilize a large distribution of measuring units, are achieved for larger distances and with a simpler setup using just three STDP-based AOA units.

OCIS codes: (200.4700) Optical neural systems; (060.5625) Radio frequency photonics; (350.4010) Microwaves; (120.0120) Instrumentation, measurement, and metrology; (070.4340) Nonlinear optical signal processing.

References and links

1. D. Rosenbluth, K. Kravtsov, M. P. Fok, and P. R. Prucnal, "A high performance photonic pulse processing device," Opt. Express **17**(25), 22767–22772 (2009).
2. M. P. Fok, D. Rosenbluth, K. Kravtsov, and P. R. Prucnal, "Lightwave neuromorphic signal processing [in the spotlight]," IEEE Signal Process. Mag. **27**(6), 160 (2010).
3. K. S. Kravtsov, M. P. Fok, P. R. Prucnal, and D. Rosenbluth, "Ultrafast all-optical implementation of a leaky integrate-and-fire neuron," Opt. Express **19**(3), 2133–2147 (2011).
4. M. P. Fok, H. Deming, M. Nahmias, N. Rafidi, D. Rosenbluth, A. Tait, Y. Tian, and P. R. Prucnal, "Signal feature recognition based on lightwave neuromorphic signal processing," Opt. Lett. **36**(1), 19–21 (2011).
5. Y. Tian, M. P. Fok, D. Rosenbluth, and P. R. Prucnal, "Asynchronous spiking neuron based on four-wave mixing and cross absorption modulation," in *Optical Fiber Communication Conference*, 2012 OSA Technical Digest Series (Optical Society of America, 2012), paper OTh3H.1.
6. M. P. Fok, Y. Tian, D. Rosenbluth, and P. R. Prucnal, "Asynchronous spiking photonic neuron for lightwave neuromorphic signal processing," Opt. Lett. **37**(16), 3309–3311 (2012).
7. M. A. Nahmias, B. J. Shastri, A. Tait, and P. R. Prucnal, "A leaky integrate-and-fire laser neuron for ultrafast cognitive computing," IEEE J. Sel. Top. Quantum Electron. **19**(5), 1–12 (2013).
8. M. P. Fok, Y. Tian, D. Rosenbluth, and P. R. Prucnal, "Pulse lead/lag timing detection for adaptive feedback and control based on optical spike-timing-dependent plasticity," Opt. Lett. **38**(4), 419–421 (2013).
9. R. C. Froemke and Y. Dan, "Spike-timing-dependent synaptic modification induced by natural spike trains," Nature **416**(6879), 433–438 (2002).
10. R. Toole and M. P. Fok, "Photonic implementation of a neuronal learning algorithm based on spike timing dependent plasticity," in *Optical Fiber Communication Conference*, 2015 OSA Technical Digest Series (Optical Society of America, 2015), paper W1K.6.
11. H. Liu, H. Darabi, P. Banerjee, and J. Liu, "Survey of wireless indoor positioning techniques and systems," IEEE Trans. Syst., Man, Cybern. C **37**(6), 1067–1080 (2007).
12. D. Niculescu and B. Nath, "Ad hoc positioning system (APS) using AOA," in *INFOCOM 2003. Twenty-Second Annual Joint Conference of the IEEE Computer and Communications* (IEEE, 2003), pp.1734–1743.
13. I. Amundson, J. Sallai, X. Koutsoukos, A. Ledeczi, and M. Maroti, "RF angle of arrival-based node localization," Int. J. Sens. Netw. **9**(3), 209–224 (2011).
14. W. Gerok, M. El-Hadidy, S. A. El Din, and T. Kaiser, "Influence of the real UWB antennas on the AOA estimation based on the TDOA localization technique," in *IEEE Middle East Conference on Antennas and Propagation* (IEEE, 2010), pp. 1–6.

#239652 - $15.00 USD Received 23 Apr 2015; revised 21 May 2015; accepted 26 May 2015; published 9 Jun 2015

15. M. C. O'Connor, "HP kicks off U.S. RFID demo center," http://www.rfidjournal.com/article/articleview/1211/1/50/.
16. A. Teuber, B. Eissfeller, and T. Pany, "A two-stage fuzzy logic approach for wireless LAN indoor positioning," in *Proc. IEEE/ION Position Location Navigat. Symp* **4** (IEEE, 2006), pp. 730–738.
17. M. Brunato and R. Battiti, "Statistical learning theory for location fingerprinting in wireless LANs," Comput. Netw. **47**(6), 825–845 (2005).
18. M. W. Khan, N. Salman, and A. H. Kemp, "Cooperative positioning using angle of arrival and time of arrival," in *Sensor Signal Processing for Defence* (IEEE, 2014), pp. 1–5.
19. N. Vo, S. Lee, and S. Challa, "Weighted nonmetric MDS for sensor localization," in *International Conference on Advanced Technologies for Communications* (IEEE, 2008), pp. 391–394.
20. X. Zou, W. Li, W. Pan, B. Luo, L. Yan, and J. Yao, "Photonic approach to the measurement of time-difference-of-arrival and angle-of-arrival of a microwave signal," Opt. Lett. **37**(4), 755–757 (2012).
21. A. Galvanauskas, P. A. Krug, and D. Harter, "Nanosecond-to-picosecond pulse compression with fiber gratings in a compact fiber-based chirped-pulse-amplification system," Opt. Lett. **21**(14), 1049–1051 (1996).
22. S. Thomas, A. Malacarne, F. Fresi, L. Potì, A. Bogoni, and J. Azaña, "Programmable fiber-based picosecond optical pulse shaper using time-domain binary phase-only linear filtering," Opt. Lett. **34**(4), 545–547 (2009).
23. L. Fu, A. Fuerbach, I. C. M. Littler, and B. J. Eggleton, "Efficient optical pulse compression using chalcogenide single-mode fibers," Appl. Phys. Lett. **88**(8), 081116 (2006).
24. A. Tait, B. J. Shastri, M. P. Fok, M. A. Nahmias, and P. R. Prucnal, "The DREAM: an integrated photonic thresholder," J. Lightwave Technol. **31**(8), 1263–1272 (2013).

1. Introduction

Neuromorphic engineering is a rapidly growing, interdisciplinary field of study in which researchers take advantage of the principles underlying biological neural networks in projects involving adaptive control, learning, sensory processing, perception, and robotics. Photonic systems, characterized by their terahertz rate signal processing and wide bandwidth, have been proven capable of implementing neuromorphic pulse processing schemes in recent years [1–8]. Perhaps the most interesting capability of neurons, the ability to learn, has been represented in photonic pulse processing systems adopting the spike timing dependent plasticity (STDP) algorithm [9]. The STDP algorithm describes the process by which the synaptic connection strength between two neurons in a network increases or decreases based on the relative timing of a neuron's inputs (presynaptic spikes) and outputs (postsynaptic spikes) [10]. In one scenario depicted by STDP, the strength of a synaptic connection is increased, a process known as "potentiation," as a presynaptic spike received by a neuron contributes to that neuron firing a postsynaptic spike. The other possible scenario, "depression," occurs when a neuron receives input after firing, and the synaptic connection is weakened. This plasticity algorithm is represented in Fig. 1(a), with Δt representing the difference between postsynaptic firing time and presynaptic reception time, and ΔW representing the resulting change in synaptic weight.

Ultrafast decision-making and adaptability at terahertz rates, speeds that are billions of times faster than those exhibited by biological systems, can be recognized when implementing this pulse processing scheme with photonics [4,8,10]. Utilizing these rates, a number of photonic-neuron circuits have been explored, including a complete neuron model, demonstration of a crayfish tail-flip escape response, and a system capable of supervised learning [1,4,8]. In this paper, a photonic implementation of STDP, through use of the nonlinear photonic effects of nonlinear polarization rotation (NPR) and cross gain modulation (XGM) within a single semiconductor optical amplifier (SOA), is experimentally demonstrated. While mimicking natural phenomena exhibited by biological systems, practical applications of these complex neural processes become apparent.

As such, we explore a photonic approach towards angle of arrival (AOA) measurement and localization of a microwave signal implementing the presented STDP circuitry. The STDP circuitry has a unique capability of determining the angle as well as the direction of arrival. AOA measurement is a powerful tool implemented in wireless localization schemes, capable of locating a microwave transmission source in three dimensions with only three measuring units [11]. In general, an AOA unit consists primarily of an antenna array, measuring the time difference of arrival (TDOA) of an incident signal to determine the angle

#239652 - $15.00 USD Received 23 Apr 2015; revised 21 May 2015; accepted 26 May 2015; published 9 Jun 2015

from which the signal arrived. AOA techniques based on ultrasound signals, RF signals, and ultra wideband (UWB) pulses have all been explored [11–17]. Localization schemes making cooperative use of various positioning techniques, such as AOA with time of arrival (TOA) and received signal strength (RSS) with TOA have also been explored [11,18,19]. Certain systems have proven capable of localization accuracies on the order of tens of centimeters, such as Hewlett Packard's smartLOCUS, utilizing an RSS and ultrasound technique, and the Ubisense and Sapphire Dart systems, both implementing UWB TDOA techniques; however, such accuracies generally require a highly complex and expensive system [11,15–17]. In recent years, a photonic AOA system was also proven powerful, yielding high accuracies, but the promising field of photonic microwave localization remains largely underdeveloped or unexplored [20]. Here, an STDP-based AOA measuring unit is simulated, and its accuracy and limitations are explored. Based on this AOA unit, a microwave transmitter localization scheme is then theoretically developed. The technique presented exhibits promise in multiple scenarios, for both use in an indoor and outdoor positioning system, depending on certain system parameters such as the spacing of the measuring units. Depending on the scale of the system, transmitters operating over a wide microwave frequency range can be located with centimeter accuracy at indoor distances of tens of meters, rivaling preexisting UWB approaches with approximately 20 cm accuracy [11].

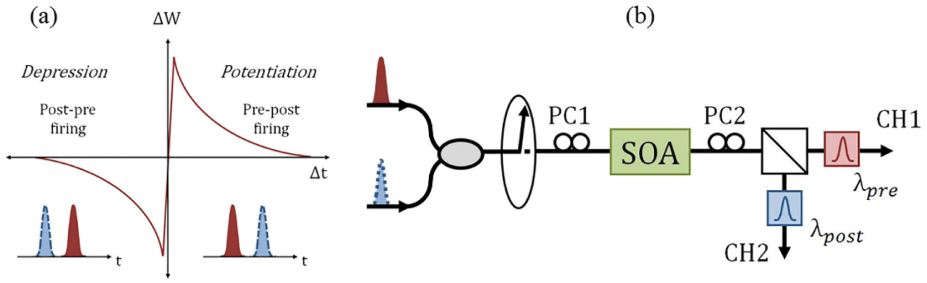

Fig. 1. (a) Theoretical STDP curve; (b) STDP experimental setup - Oval with arrow: polarizer; PC1 and PC2: polarization controllers; SOA: semiconductor optical amplifier; Square with diagonal: polarization beam splitter; Colored squares: bandpass filters at λ_{pre} and λ_{post}.

2. Photonic implementation of STDP

2.1. Principle and experimental setup

The experimental setup for optical STDP realization is shown in Fig. 1(b). The STDP circuit is a relatively simple system that mainly consists of a single semiconductor optical amplifier (SOA), two bandpass filters, and a polarization beam splitter (PBS). A polarizer and polarization controllers (PCs) are used for initial polarization alignment before operation. To experimentally verify generation of the STDP characteristic, two optical pulses at different wavelengths are generated using a fiber laser and four-wave mixing (FWM) and sent through the STDP circuitry at various time delays [10]. The pre- and postsynaptic (red and dashed blue, respectively) optical spike trains, at 1550.12 nm (λ_{pre}) and 1553.33 nm (λ_{post}), respectively, maintain a repetition rate of 625 MHz at an average power of –4 dBm. Both spikes enter into the STDP circuit in the same polarization state, and a 600 ps variable optical delay line is inserted into the presynaptic branch to implement tunable time delay between the spikes.

The delay is initialized such that the postsynaptic spike precedes the presynaptic spike by over 300 ps, and PC1, as labeled in Fig. 1(b), is adjusted so that the input pulses experience the highest possible, equivalent gain at maximum separation. At a time difference of 300 ps, with t_{post} being significantly less than t_{pre}, the SOA has adequate time to recover between inputs, and each pulse experiences the same level of amplification and the same minimal polarization rotation, allowing for PC2 to be properly initialized. This PC is adjusted so that

#239652 - $15.00 USD Received 23 Apr 2015; revised 21 May 2015; accepted 26 May 2015; published 9 Jun 2015

the SOA output is initially aligned to one channel of the PBS, channel 1 (CH1), minimizing the throughput of channel 2 (CH2). Next, the delay is adjusted so that $\Delta t = t_{post} - t_{pre}$ ranges from 300 to −300 ps, and the output power of both channels is combined and measured at different delays to construct the STDP curve.

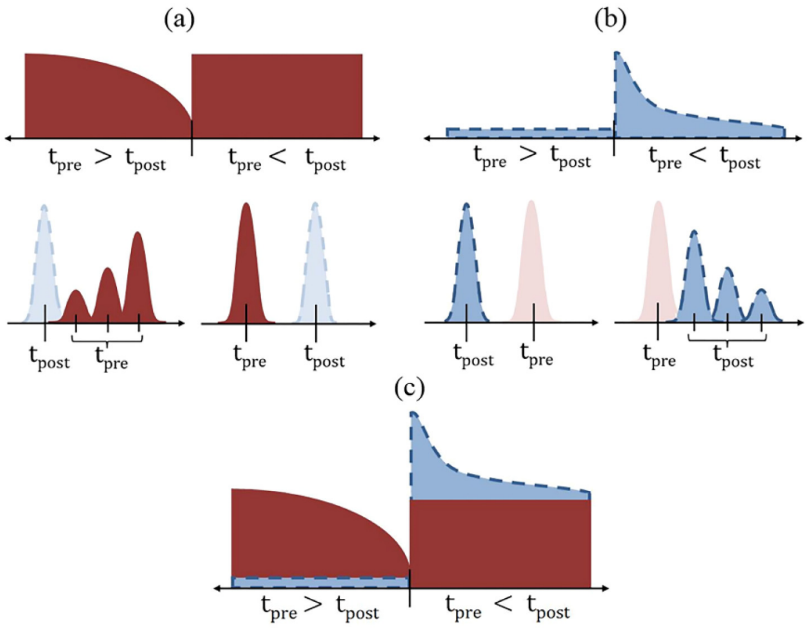

Fig. 2. (a) Photonic STDP channel 1 output; (b) Channel 2 output; (c) Channels 1 and 2 combined.

Figure 2 illustrates the means through which the depression and potentiation windows of the STDP response are generated. As shown by Fig. 2(a), a gain depletion response of CH1 at the λ_{pre} wavelength is responsible for acquisition of the depression window. When a pulse enters the SOA and depletes the device's gain, the trailing pulse experiences minimal amplification. For Δt values below zero, corresponding to the left side of Fig. 2(a), the postsynaptic spike (dashed blue) precedes the presynaptic spike (solid red), and, if the time difference is small, the SOA has little time to recover. Consequently, the presynaptic spike experiences almost no amplification. As Δt becomes more negative, the spacing increases, and the SOA has more time to recover. This allows for the presynaptic spike to experience higher levels of amplification and results in the generation of the depression window, seen on the left side of Fig. 2(a). If Δt is greater than zero, the leading presynaptic spike experiences the same maximum level of amplification across the entire range of positive Δt values and experiences no XGM, resulting in the right side of Fig. 2(a).

As illustrated by the left side of Fig. 2(b), for all negative Δt values, the preceding postsynaptic spike experiences no NPR, and the CH2 output at λ_{post} remains constant. When the postsynaptic spike follows shortly behind the presynaptic spike, however, the trailing spike experiences NPR due to the birefringence change in the SOA induced by the presynaptic spike. The effect is strongest for small Δt and decreases as Δt increases; thus, the right side of Fig. 2(b) is realized. As indicated by Fig. 2(c), the linearly combined power outputs of channels 1 and 2 for all values of Δt between −300 and 300 ps generate the STDP curve.

#239652 - $15.00 USD Received 23 Apr 2015; revised 21 May 2015; accepted 26 May 2015; published 9 Jun 2015

2.2. Results and discussion

Prior to the full realization of the photonic STDP curve, the cooperative effects of XGM and NPR were exhibited in a simple experiment with a 1540.6 nm pulse pump and a 1550.12 nm CW probe. In the same polarization state, the CW signal and the pulse train, with 10 ps pulse widths and a 625 MHz repetition rate, were sent through an SOA and a PBS, with a 1550.12 nm bandpass filter and photodetector (PD) in each branch. Both XGM and NPR effects happen simultaneously in the SOA and the results are observed at each of the outputs of the PBS, CH1 and CH2, respectively. The resulting oscilloscope traces of both branches of the PBS are shown in Fig. 3(a). The XGM and NPR effects are exhibited by the green curve (bottom) and yellow curve (top), respectively, illustrating the feasibility of obtaining both STDP windows with a single SOA.

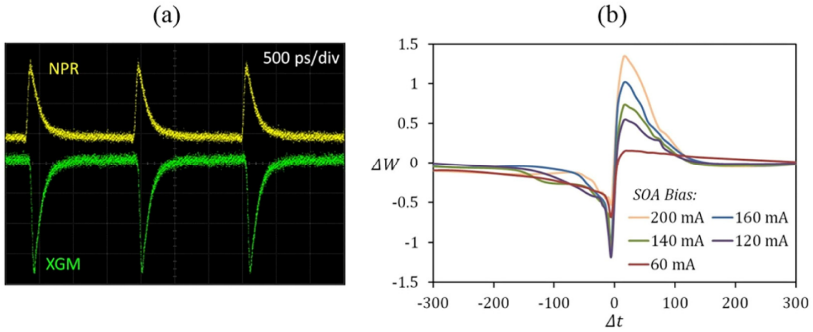

Fig. 3. (a) Oscilloscope traces of preliminary NPR and XGM results. (b) Experimental STDP results given different SOA driving currents.

Figure 3(b) displays the experimental results of the complete STDP experiment, with both pre- and postsynaptic spikes. Considering the low power of CH2, the NPR channel, amplification by 15 dBm was necessary to acquire depression and potentiation windows with similar magnitudes. The normalized STDP curves at various SOA driving currents are presented. Evidently, control over the shape of both windows is achievable by tuning the SOA driving current. As driving current increases, the peak of the potentiation window increases, due to the increase in birefringence induced by higher-amplified pulses; however, the width of the potentiation window remains relatively constant, likely due to the fact that higher driving currents result in quicker restoration of the device's original birefringence. The increasing NPR response and decreasing recovery time compete, serving to maintain the potentiation window's width across increasing driving currents. As for the depression window, increasing the driving current and consequently decreasing the recovery time, serves to decrease the window's width, while maintaining the depth over increasing driving currents. The presented method of producing an STDP response can be used to demonstrate ultrafast learning in a photonic neuron, as presented in other works with different STDP setups [8].

3. STDP-based AOA localization

3.1. Principle and theoretical setup

One of the motivations in exploring neuromorphic engineering systems is the possibility of discovering novel techniques or algorithms that prove useful in advancing other engineering applications. One such manifestation of this motivation, the STDP-inspired AOA system, is presented in this letter. The proposed system, shown in Fig. 4(a), consists primarily of two CW sources at λ_{pre} and λ_{post}, two Mach-Zehnder modulators (MZMs), two microwave antennae, and the described STDP system. A microwave signal at a frequency f_{RF} is emitted by a transmitter, and is received by two antennas at the AOA circuit, passing through impulse generators and arriving at each MZM. Due to the path difference between the transmitter and

#239652 - $15.00 USD Received 23 Apr 2015; revised 21 May 2015; accepted 26 May 2015; published 9 Jun 2015

each of the two antennas, the received signal experiences different phase shifts (i.e. time delay) at each antenna. Upon modulation, two optical pulse trains with f_{RF} repetition rates are sent into the STDP system. If the optical pulse widths aren't sufficiently small, a number of different methods could be implemented to compress the pulses, depending on f_{RF} and the impulse generators [21–23]. The initial phase difference of the received microwave signals translates to a time delay between optical pulses entering into the STDP system. The STDP circuit produces a unique power output for negative and positive values of Δt, ranging from $-t_m = -d/c$ to t_m, where d is the antenna spacing, and c is the propagation speed. The ability of producing a unique output for both negative and positive values of Δt eliminates the ambiguity arising from the measurement of signals arriving from opposite directions but at the same angle relative to the antenna array. Consequently, angles between 0° and 180°, corresponding to delays of $\pm t_m$, are distinguishable in this AOA scenario. The measured angle θ of an AOA array is indicated in the Fig. 4(a) inset, corresponding to different time delays Δt. The normalized STDP output corresponds to a particular delay, which is used to determine the angle through the simple relationship, $c \cdot \Delta t = d \cdot \cos\theta$.

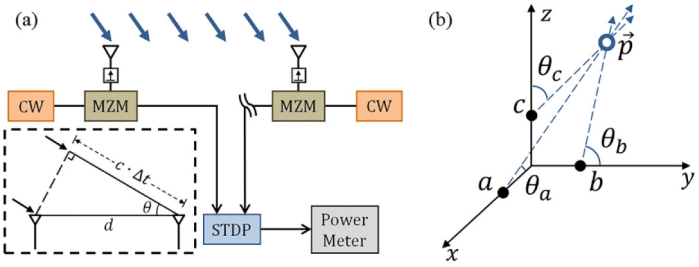

Fig. 4. (a) STDP AOA array, with AOA response depicted in the inset; (b) Basic 3D AOA localization schematic with three nodes uncovering three directions, θ_a, θ_b, θ_c.

It should also be noted that the operating frequency range of an AOA array is limited by the antenna spacing, d. Considering the periodic nature of the received signal, the maximum possible signal frequency is determined by the relationship, $f_m = c/2 \cdot d$, where f_m is the maximum frequency. For any higher frequency, the STDP circuit is not guaranteed to perform its measurement on the proper set of two pulses, as ambiguity exists between which pulse is "pre" and "post" in a continuous pulse train. The previously explained STDP setup is limited to frequencies below approximately 1.66 GHz, with d at 9 cm. To achieve higher operating frequencies, the antenna spacing can be decreased, provided that the resulting Δt values are greater than the SOA recovery time.

Furthermore, this individual AOA measuring unit shows promise in being implemented in a 3D localization scheme, as depicted in Fig. 4(b). The primitive, simulated system consists of three STDP-based AOA arrays, each positioned on a Cartesian axis at $(x_a,0,0)$, $(0,y_b,0)$, and $(0,0,z_c)$ at points a, b, and c respectively. Each array's AOA value, θ_a, θ_b, and θ_c, contributes to constructing a simple set of nonlinear equations, three conical surfaces, shown below,

$$\left(x_0 - x_a\right)^2 = \cot^2\theta_a \cdot \left({y_0}^2 + {z_0}^2\right), \tag{1}$$

$$\left(y_0 - y_b\right)^2 = \cot^2\theta_b \cdot \left({x_0}^2 + {z_0}^2\right), \tag{2}$$

$$\left(z_0 - z_c\right)^2 = \cot^2\theta_c \cdot \left({x_0}^2 + {y_0}^2\right), \tag{3}$$

#239652 - $15.00 USD Received 23 Apr 2015; revised 21 May 2015; accepted 26 May 2015; published 9 Jun 2015

from which a microwave transmitter's location at (x_0,y_0,z_0) can be determined. Two primary sources of error, measuring unit location error and laser instability, are considered in the AOA and 3D localization simulations.

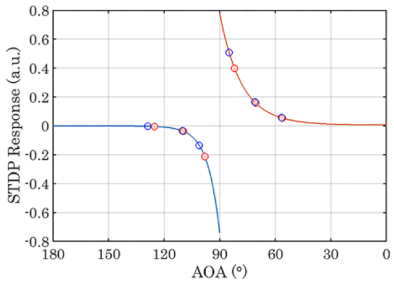

Fig. 5. Comparison of expected (red) and observed (blue) STDP outputs for nodes at x_a = 0.5, 5, 8, 12, 15, and 20 m.

3.2 Results and discussion

For the AOA system simulation, the STDP measuring unit is receiving a microwave signal from a transmitter at known location, (x_0,y_0,z_0), in meters. Figure 5 illustrates the expected (red filled) and observed (blue outlined) STDP output for a node at x_a = 0.5, 5, 8, 12, 15, and 20 m, with the furthest right pair corresponding to x_a = 0.5 m, and the furthest left pair corresponding to x_a = 20 m. The expected (red) points represent ideal outputs free of error, and the blue points represent outputs when the system is subjected to error. The transmitter is located at an arbitrary point, (10,10,10), and error in the form of unit displacement and laser power fluctuations is considered. For an indoor wireless localization system, unit displacement would be low, so a 1 mm error is considered. The other contribution to the error of the observed STDP output is 0.003 dBm of laser power error, as the DFB laser used for CW generation in our STDP experiments claims such levels of power instability. The results depict the AOA error for different angles, indicating larger expected errors for angles near to 0°, 90°, and 180°.

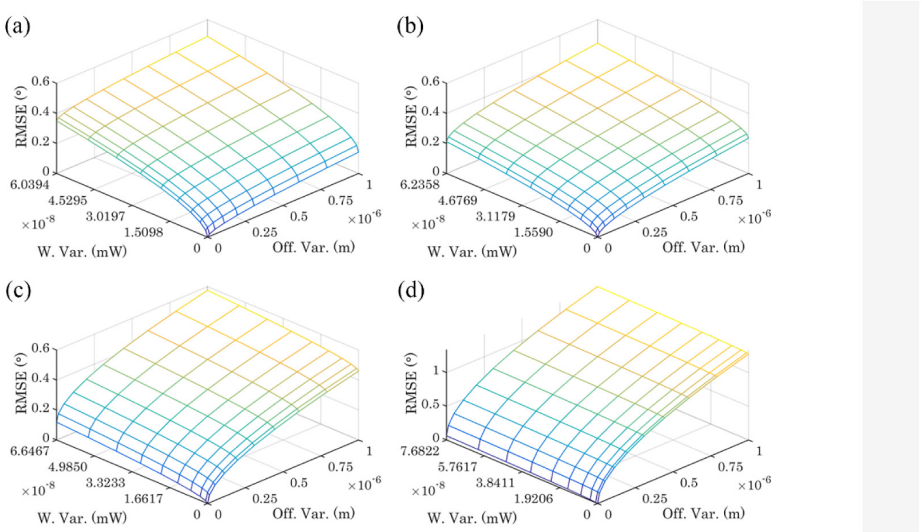

Fig. 6. (a) Error plot for an AOA node at (1,0,0) detecting a transmitter at (10,10,10); (b) AOA error plot for a node at (3,0,0); (c) AOA error plot for a node at (5,0,0); (d) AOA error plot for a node at (7,0,0).

#239652 - $15.00 USD Received 23 Apr 2015; revised 21 May 2015; accepted 26 May 2015; published 9 Jun 2015

The device's performance in locating a transmitter at the same point, (10,10,10), is shown in Fig. 6, which illustrates error plots for the unit's AOA measuring ability when considering a range of unit displacement and laser power fluctuations of up to 1 mm and 0.003 dBm, respectively. Each error plot presents the root mean square error (RMSE) of the device's AOA measurement in degrees, with respect to variance in the forms explained above. As illustrated in Fig. 6(a), even with maximum variance in both node location and laser power, the relative AOA measurement errors for a measuring unit located at (1,0,0) and a transmitter located at (10,10,10), both in meters, do not exceed 0.5°. Furthermore, by relocating the node to (3,0,0), illustrated by Fig. 6(b), the maximum RMSE can be decreased to approximately 0.425°. As the detected AOA approaches 90°, measurement error due to laser instability continues to decrease while error due to offset variance begins to dominate, shown by Figs. 6(c) and 6(d) for nodes at (5,0,0) and (7,0,0). For each of the four scenarios, the STDP AOA array outperforms previously explored photonics-based AOA devices, which report errors of ± 2.5° [20].

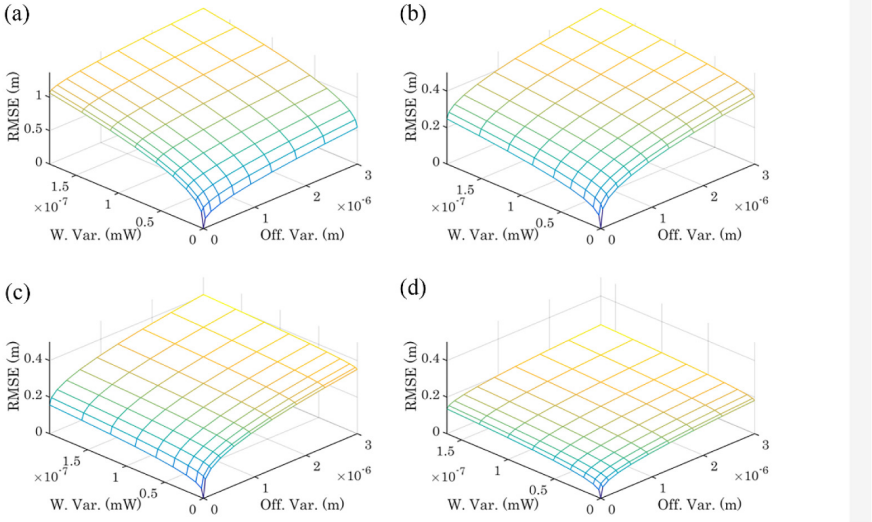

Fig. 7. (a) Error plot for detecting a transmitter at (10,10,10) with nodes at $x_a = y_b = z_c = 1$ m; (b) Error plot with nodes at $x_a = 1$ m, $y_b = z_c = 5$ m; (c) Error plot for nodes at $x_a = y_b = z_c = 5$ m; (d) Error plot for nodes at $x_a = y_b = z_c = 15$ m.

The error plots for the full 3D localization scheme are presented in Fig. 7. With a maximum location error of 1 mm and laser instability of 0.003 dBm for each node, the RMSE, in meters, of the transmitter location is at most just over 1 m, occurring when the AOA arrays are located at $x_a = y_b = z_c = 1$ m. By relocating two of the nodes to $y_b = z_c = 5$ m, the maximum RMSE is decreased to 0.4 m. Considering the same error values and nodes at $x_a = y_b = z_c = 5$ m, a maximum RMSE of about 0.3 m is acquired and can be reduced even further to 0.15 m by positioning the nodes at $x_a = y_b = z_c = 15$ m. The measurements report accuracies that rival that of the most accurate indoor positioning systems, which are all significantly more complex and expensive than the photonic setup presented, with their large networks of measuring units [15–17]. The presented setup relies solely on the three measuring units and achieves comparative accuracies for much larger distances between transmitters and receivers. Beyond the indoor realm, a RMSE of 9.7 m is possible with nodes located at $x_a = y_b = z_c = 5$ m, given the same error sources, when detecting a transmitter at over 100 m. This reasonable error indicates the possibility of developing such a device for outdoor positioning purposes as well.

#239652 - $15.00 USD Received 23 Apr 2015; revised 21 May 2015; accepted 26 May 2015; published 9 Jun 2015

4. Conclusion

The biological STDP algorithm has been successfully demonstrated optically using XGM and NPR cooperatively in a single SOA, and the device presented could be implemented in previously developed photonic learning systems. Furthermore, these primitive simulations illustrate the potential application of STDP photonic systems in AOA localization schemes. By solving simple nonlinear equations constructed from AOA information drawn from relatively simple photonic systems, tolerable localization accuracy is acquired for a range of transmitter distances of up to 100 m, when considering reasonable error sources and different node arrangements. Devising a highly accurate AOA system can be difficult due to the challenges presented by shadowing or multipath reflection. For a photonic system however, another technique often employed in photonic neuromorphic systems could be implemented to overcome these difficulties. Through use of an optical thresholder, all incident signals below a particular threshold could be effectively suppressed, without affecting the desirable ones [1–7,24]. All detected signals resulting from multipath reflection would be weaker than the desirable signal and consequently eliminated. Considering the role that node location relative to transmitter location plays in AOA accuracy, a modified system with a larger distribution of measuring units would exhibit higher accuracy and provide uniform precision for transmitter localization within the region.

Acknowledgments

This work is supported by National Science Foundation (Award number: ECCS 1342177, and CMMI 1400100).

#239652 - $15.00 USD Received 23 Apr 2015; revised 21 May 2015; accepted 26 May 2015; published 9 Jun 2015